Sarjonen, R.; Törmä, Päivi

Topological States with Broken Translational and Time-Reversal Symmetries in a Honeycomb-Triangular Lattice

Published in:
Physical Review A

DOI:
10.1103/PhysRevA.91.063605

Published: 01/06/2015

Document Version
Publisher's PDF, also known as Version of record

Please cite the original version:
Sarjonen, R., & Törmä, P. (2015). Topological States with Broken Translational and Time-Reversal Symmetries in a Honeycomb-Triangular Lattice. *Physical Review A*, *91*(6), 1-8. Article 063605.
https://doi.org/10.1103/PhysRevA.91.063605

Topological states with broken translational and time-reversal symmetries in a honeycomb-triangular lattice

R. Sarjonen and P. Törmä*

COMP Centre of Excellence, Department of Applied Physics, Aalto University, FI-00076 Aalto, Finland

(Received 23 September 2014; revised manuscript received 15 January 2015; published 5 June 2015)

We study fermions in a lattice, with on-site and nearest neighbor attractive interactions between two spin species. We consider two geometries: (1) both spins in a triangular lattice and (2) a mixed geometry with up spins in honeycomb and down spins in triangular lattices. We focus on the interplay between spin-population imbalance, on-site and valence bond pairing, and order parameter symmetry. The mixed geometry leads to a rich phase diagram of topologically nontrivial phases. In both geometries, we predict order parameters with simultaneous time-reversal and translational symmetry breaking.

DOI: 10.1103/PhysRevA.91.063605 PACS number(s): 67.85.−d, 71.10.Fd, 74.20.−z

I. INTRODUCTION

In the Bardeen, Cooper, and Schrieffer (BCS) theory [1], which describes well many low-temperature superconductors, the transition to the superconducting state is characterized by the breaking of gauge symmetry only. However, the hallmark of unconventional superconductivity is the breaking of additional symmetries. For example, the Fulde-Ferrel-Larkin-Ovchinnikov (FFLO) state has broken translational symmetry: The order parameter has a nontrivial spatial dependence [2–5]. On the other hand, chiral superconductors break time-reversal symmetry (TRS) because they feature gap parameters that wind in phase around the Fermi surface in multiples of 2π. Chiral superconductors also exhibit many other fascinating properties that are highly sought after for nanoscience applications [6–10], and broken TRS is a prerequisite for the quantum Hall effects (excluding the spin Hall effect) [11,12]. Moreover, in MgB_2 and iron pnictides [13–16] TRS may be broken due to interband couplings [17–19]. In this paper, we propose and theoretically study a system in which exotic superfluids with translational and TRS breaking can compete and even coexist.

Simultaneous breaking of multiple symmetries is an intriguing phenomenon; an example of a sought-after state is the supersolid which breaks translational and U(1) symmetries by coexisting crystal structure and superfluidity [20]. As another example, it was recently predicted for spinless fermions in a triangular lattice that density orders with several broken symmetries may coexist [21]. Each broken symmetry typically generates characteristic modes, the coexistence of which leads to rich physics and potential applications. Achieving such states is, however, nontrivial since the system must be susceptible to different types of order. The translational and TRS-breaking superfluids that we predict here are of conceptual interest as a type of state with simultaneous breaking of several symmetries, all reflected in the superfluid order parameter. Importantly, the very ingredients that are essential for creating such states, namely a combination of long-range interactions, special lattice geometries, and spin-density imbalance, are an emerging experimental reality in ultracold gas systems.

A crucial extension to the capabilities of ultracold Fermi gases as a quantum simulator [22,23], including emulation of the extended Fermi-Hubbard model [24–28], is emerging from the possibilities of realizing not only on-site but also long-range interactions. They can be realized, for example, with the help of atoms with a large magnetic dipole moment (e.g., chromium, dysprosium, and erbium [29–31]), dipolar molecules such as the fermionic $^{40}K^{87}Rb$ [32–34], or atoms excited to Rydberg states [35–38]. Another type of possibility is mixtures of bosonic and fermionic atoms where the bosons induce a long-range interaction between the fermions [39]. Intriguingly, ultracold gas lattice systems also enable spin-dependent confinement of particles [40–43]. This has led to theoretical proposals of new concepts, such as mixed geometry pairing [44].

II. MODEL

We consider two different lattice systems, namely a honeycomb-triangular and a triangular lattice loaded with spin-1/2 fermions. In the former system, the honeycomb lattice comprises two triangular sublattices A and B, as shown in Fig. 1(a). The sublattices are spin selective in such a way that $\uparrow$-spin atoms can occupy the whole honeycomb lattice, but $\downarrow$-spin atoms are confined to the triangular sublattice A. Consequently, we denote the honeycomb lattice by $\mathcal{L}_\uparrow$ and the triangular sublattice A by $\mathcal{L}_\downarrow$.

We assume that $\uparrow$-spin and $\downarrow$-spin atoms can tunnel only between neighboring sites of $\mathcal{L}_\uparrow$ and $\mathcal{L}_\downarrow$, respectively. We denote the tunneling amplitudes of $\uparrow$-spin and $\downarrow$-spin atoms by $t_\uparrow$ and $t_\downarrow$, respectively. Subsequently, the Hamiltonian that takes into account tunneling and possible on-site energy modulations can be written as

$$\mathcal{H}_0 = -t_\uparrow \sum_{\langle i,j\rangle\in\mathcal{L}_\uparrow} (\hat{a}^\dagger_{i\uparrow}\hat{b}_{j\uparrow} + \text{H.c.}) - \mu_\uparrow \sum_i \left(\hat{n}^a_{i\uparrow} + \hat{n}^b_{i\uparrow}\right) - t_\downarrow \sum_{\langle i,j\rangle\in\mathcal{L}_\downarrow} (\hat{a}^\dagger_{i\downarrow}\hat{a}_{j\downarrow} + \text{H.c.}) - (\mu_\downarrow - \epsilon^a_\downarrow)\sum_i \hat{n}^a_{i\downarrow}, \quad (1)$$

where $\hat{a}^\dagger$ ($\hat{a}$) and $\hat{b}^\dagger$ ($\hat{b}$) are fermionic creation (annihilation) operators in sublattices A and B, respectively, and $\hat{n}^a$ and $\hat{n}^b$ are the corresponding density operators. Parameters $\mu_\uparrow$ and $\mu_\downarrow$ are chemical potentials for $\uparrow$-spin and $\downarrow$-spin particles, respectively. In order to make our results comparable with the

*Corresponding author: paivi.torma@aalto.fi

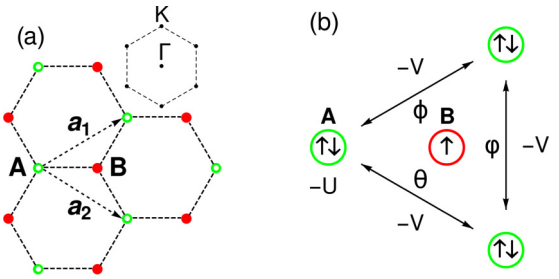

FIG. 1. (Color online) Schematic representation of honeycomb-triangular lattice. (a) Honeycomb-triangular lattice and its Brillouin zone. Sublattice A (green [light gray]) houses both spins, whereas sublattice B (red [dark gray]) houses only up-spin paricles. (b) Pairing happens both on site and intersite with energy gains $-U$ and $-V$, respectively. Phases of the bond order parameters are marked with θ, ϕ, and φ.

ones in Ref. [44], we choose $\epsilon^a_\downarrow = -3$, and set $t_\uparrow = t_\downarrow = t = 1$ in all our calculations.

Here we focus on pairing and types of superfluidity that arise from attractive interactions. In experiments, there are many ways to tune the interparticle interactions from attractive to repulsive, such as Feshbach resonances [45]. Moreover, there are ways to tune the on-site and nearest-neighbor (NN) interactions independently of each other [46,47]. Thus, we choose to consider attractive on-site and nearest-neighbor interactions. The on-site interaction takes place at A sites, and we denote the interaction strength by $-U$ where $U \geqslant 0$. The corresponding Hamiltonian reads

$$\mathcal{H}_{\rm os} = -U \sum_j \hat{n}^a_{j\uparrow} \hat{n}^a_{j\downarrow}. \tag{2}$$

In conventional superconductivity, electrons form superconducting Cooper pairs in a spin-singlet state [48]. However, spin-singlet bonding between neighboring A and B sites is impossible because $\downarrow$-spin particles cannot occupy B sites. Therefore we assume that the nearest neighbor interaction takes place between adjacent A sites and represent it with the Hamiltonian

$$\mathcal{H}_{\rm nn} = -V \sum_{\langle m,n\rangle \in \mathcal{L}_\downarrow} \hat{h}^\dagger_{mn} \hat{h}_{mn}, \tag{3}$$

where $\hat{h}^\dagger_{mn} = (\hat{a}^\dagger_{m\uparrow}\hat{a}^\dagger_{n\downarrow} - \hat{a}^\dagger_{m\downarrow}\hat{a}^\dagger_{n\uparrow})/\sqrt{2}$ is a spin-singlet creation operator. The parameter $V > 0$ represents an energy gain when two atoms form a spin-singlet bond, because $\hat{h}^\dagger_{mn}\hat{h}_{mn}$ is the number operator for singlet bonds [49]. We note that the spin-singlet states between neighboring sites are essentially resonating-valence-bond states proposed by Anderson [50].

The full Hamiltonian for the honeycomb-triangular lattice is

$$\mathcal{H} = \mathcal{H}_0 + \mathcal{H}_{\rm os} + \mathcal{H}_{\rm nn}. \tag{4}$$

We treat the interaction terms $\mathcal{H}_{\rm os}$ and $\mathcal{H}_{\rm nn}$ in the mean-field (MF) approximation. As we employ fermionic anticommutation relations and ignore the Hartree shifts, we obtain the MF Hamiltonians

$$\mathcal{H}^{\rm MF}_{\rm os} = -U \sum_j \langle \hat{a}_{j\downarrow}\hat{a}_{j\uparrow}\rangle \hat{a}^\dagger_{j\uparrow}\hat{a}^\dagger_{j\downarrow} + \text{H.c.} - |\langle \hat{a}_{j\downarrow}\hat{a}_{j\uparrow}\rangle|^2, \tag{5}$$

$$\mathcal{H}^{\rm MF}_{\rm nn} = -V \sum_{\langle m,n\rangle \in \mathcal{L}_\downarrow} \langle \hat{h}_{mn}\rangle \hat{h}^\dagger_{mn} + \text{H.c.} - |\langle \hat{h}_{mn}\rangle|^2. \tag{6}$$

In the model of Ref. [44] the possibility of FFLO phase was not considered: There were forbidden areas in the phase diagrams, which usually suggest that the mean-field ansatz has been limited. Here we want to consider also the possibility of symmetry-breaking superfluid phases, and therefore we take into account the possibility that Cooper pairs have nonzero center-of-mass momenta. Consequently, we use an FFLO-type ansatz $U\langle \hat{a}_{j\downarrow}\hat{a}_{j\uparrow}\rangle = \Delta_0 e^{2i\mathbf{q}\cdot\mathbf{x}_j}$ [51] for the on-site order parameter. Here $\mathbf{x}_j$ is the position vector of lattice site j, amplitude $\Delta_0 \geqslant 0$, and $2\mathbf{q}$ is the Cooper pair center-of-mass momentum. On the other hand, there are three different NN bonds on a triangular lattice. We take the three different NN bonds to be along directions $\mathbf{a}_2$, $\mathbf{a}_1$, and $\mathbf{a}_1 - \mathbf{a}_2$ specified in Figs. 1(a) and 1(b). We consider a simple situation in which the long-range order parameter has the same norm Δ_1 along all bonds, but different phases are allowed for the different bonds [52]. In equation form, the ansatz reads $V\langle \hat{h}_{mn}\rangle = \Delta_1 e^{i\theta_{mn}} e^{i\mathbf{q}\cdot(\mathbf{x}_m+\mathbf{x}_n)}$, where $\Delta_1 \in \mathbb{R}$ and θ_{mn} is the phase that depends on the direction of the bond between sites m and n. We denote the phases corresponding to bonds $\mathbf{a}_2$, $\mathbf{a}_1$, and $\mathbf{a}_1 - \mathbf{a}_2$ by θ, ϕ, and φ, respectively.

We define the Fourier transformation as $\tilde{f}_{\mathbf{k}\sigma} = M^{-1/2}\sum_j e^{-i\mathbf{k}\cdot\mathbf{x}_j}\hat{f}_{j\sigma}$, where $f \in \{a,b\}$, $\sigma \in \{\uparrow,\downarrow\}$, and M is the number of sites in either of the triangular sublattices A and B. With the help of the Fourier transformation and periodic boundary conditions in real space, the mean-field Hamiltonian can be written in momentum space as

$$\mathcal{H}^{\rm MF} = \sum_{\mathbf{k}} \tilde{\Psi}^\dagger_{\mathbf{k}} \mathcal{H}_{\mathbf{k}} \tilde{\Psi}_{\mathbf{k}} + \frac{3|\Delta_1|^2}{V} + \frac{|\Delta_0|^2}{U} + \xi^{(3)}_{-\mathbf{k}}, \tag{7}$$

where

$$\tilde{\Psi}_{\mathbf{k}} = \begin{pmatrix} \hat{c}^{(1)}_{\mathbf{k}} & \hat{c}^{(2)}_{\mathbf{k}} & \hat{c}^{(3)\dagger}_{2\mathbf{q}-\mathbf{k}} \end{pmatrix}^{\rm T} \tag{8}$$

and [53]

$$\mathcal{H}_{\mathbf{k}} = \begin{pmatrix} \xi^{(1)}_{\mathbf{k}} & 0 & g^*_{\mathbf{k}} + \mathcal{G}^*_{\mathbf{k}-\mathbf{q}} \\ 0 & \xi^{(2)}_{\mathbf{k}} & g^*_{\mathbf{k}} + \mathcal{G}^*_{\mathbf{k}-\mathbf{q}} \\ g_{\mathbf{k}} + \mathcal{G}_{\mathbf{k}-\mathbf{q}} & g_{\mathbf{k}} + \mathcal{G}_{\mathbf{k}-\mathbf{q}} & -\xi^{(3)}_{2\mathbf{q}-\mathbf{k}} \end{pmatrix}. \tag{9}$$

The noninteracting dispersions are explicitly written as $\xi^{(1,2)}_{\mathbf{k}} = \pm|h_\uparrow(\mathbf{k})| - \mu_\uparrow$, where $h_\uparrow(\mathbf{k}) = -t_\uparrow[e^{ik_x/\sqrt{3}} + 2e^{-ik_x/(2\sqrt{3})}\cos(k_y/2)]$ and $\xi^{(3)}_{\mathbf{k}} = -t_\downarrow(2[\cos k_y + \cos([k_y + \sqrt{3}k_x]/2) + \cos([k_y - \sqrt{3}k_x]/2)] + 3) - \mu_\downarrow$. The interband coupling due to the on-site interaction is $g_{\mathbf{k}} = -\Delta_0/\sqrt{2}$. Similarly, the interband coupling due to the NN interaction is $\mathcal{G}_{\mathbf{k}-\mathbf{q}} = -\Delta_1\sum_\delta e^{-i\Theta_\delta}\cos([\mathbf{k}-\mathbf{q}]\cdot\boldsymbol{\delta})$, where $\sum_\delta$ goes over the nearest neighbors $\mathbf{a}_2$, $\mathbf{a}_1$, and $\mathbf{a}_1 - \mathbf{a}_2$, and Θ_δ is the phase corresponding to $\boldsymbol{\delta}$.

As mentioned in the introduction, we also consider a triangular lattice spanned by the primitive vectors $\mathbf{a}_1$ and $\mathbf{a}_2$. We describe tunneling and possible on-site energy modulations

with the Hamiltonian

$$H_0 = -t_\uparrow \sum_{\langle i,j\rangle} (\hat{a}^\dagger_{i\uparrow}\hat{a}_{j\uparrow} + \text{H.c.}) - t_\downarrow \sum_{\langle i,j\rangle} (\hat{a}^\dagger_{i\downarrow}\hat{a}_{j\downarrow} + \text{H.c.}) - \mu_\uparrow \sum_i \hat{n}^a_{i\uparrow} - (\mu_\downarrow - \tilde{\epsilon}^a_\downarrow) \sum_i \hat{n}^a_{i\downarrow} \quad (10)$$

and choose $\tilde{\epsilon}^a_\downarrow = 0$ in all subsequent calculations. The on-site and nearest neighbor interaction terms for the triangular and honeycomb-triangular lattices are the same. Thus the full Hamiltonian for the triangular lattice is $H = H_0 + \mathcal{H}_{\text{os}} + \mathcal{H}_{\text{nn}}$. Subsequently, with the help of Fourier transformation we obtain

$$H^{\text{MF}} = \sum_{\mathbf{k}} \tilde{\psi}^\dagger_{\mathbf{k}} H_{\mathbf{k}} \tilde{\psi}_{\mathbf{k}} + \frac{3|\Delta_1|^2}{V} + \frac{|\Delta_0|^2}{U} + E^{(2)}_{\mathbf{k}}, \quad (11)$$

where

$$\tilde{\psi}_{\mathbf{k}} = (\tilde{a}_{\mathbf{k}\uparrow} \quad \tilde{a}^\dagger_{2\mathbf{q}-\mathbf{k},\downarrow})^{\text{T}} \quad (12)$$

and

$$H_{\mathbf{k}} = \begin{pmatrix} E^{(1)}_{\mathbf{k}} & -\Delta^*_0 + \mathcal{G}^*_{\mathbf{k}-\mathbf{q}} \\ -\Delta_0 + \mathcal{G}_{\mathbf{k}-\mathbf{q}} & -E^{(2)}_{2\mathbf{q}-\mathbf{k}} \end{pmatrix}. \quad (13)$$

The noninteracting energy dispersions are

$$E^{(1)}_{\mathbf{k}} = E_{\mathbf{k}} - \mu_\uparrow, \quad (14)$$

$$E^{(2)}_{\mathbf{k}} = E_{\mathbf{k}} - \mu_\downarrow, \quad (15)$$

where

$$E_{\mathbf{k}} = -2\left[\cos k_y + \cos\left(\frac{k_y + \sqrt{3}k_x}{2}\right) + \cos\left(\frac{k_y - \sqrt{3}k_x}{2}\right)\right]. \quad (16)$$

When interaction strengths and tunneling amplitudes are fixed, the parameters that govern pairing in the system are the chemical potentials $\mu_\uparrow$ and $\mu_\downarrow$. The grand potential is defined as $\Omega = (-1/\beta)\ln \text{Tr}\, e^{-\beta \hat{H}}$, where $\hat{H} \in \{\mathcal{H}^{\text{MF}}, H^{\text{MF}}\}$ and $\beta = 1/(k_{\text{B}}T)$ with k_{B} being the Boltzmann constant and T being the temperature. The location of the absolute minimum of the grand potential $\Omega = \Omega(\Delta_0, \Delta_1, \mathbf{q})$ determines the values of Δ_0, Δ_1 and $\mathbf{q}$ [44]. Furthermore, the quasiparticle energies $E_\alpha(\mathbf{k})$, $\alpha \in \{1,2,3\}$, are given by the eigenvalues of the matrices $\mathcal{H}_{\mathbf{k}}$ and $H_{\mathbf{k}}$.

A particularly promising way to experimentally realize this model would be to employ the widely used rubidium-potassium mixture composed of fermionic ^{40}K prepared in the $|F = 9/2, m_F = -7/2\rangle$ and $|F = 9/2, m_F = -9/2\rangle$ Zeeman components of the $F = 9/2$ ground-state hyperfine level and bosonic ^{87}Rb atoms in the $|F = 1, m_F = 1\rangle$ ground state. The on-site and NN interactions could be tuned independently [54], and various experimental methods are available to study the nature of the pairing [55]. In particular, the experimental realization of the NN interaction term $\mathcal{H}_{\text{nn}}$ in ultracold Bose-Fermi mixtures has been discussed in Secs. II, III A, and III C of Ref. [39].

In units of $-(e^2/h)$, the Hall conductance of a filled band is an integer called the Chern number [12]. If we assume that the pseudospin indices $\uparrow$ and $\downarrow$ are associated with internal angular momenta, as opposed to some other internal states unaffected by time reversal, the Hamiltonian $\mathcal{H}$ is not symmetric under time reversal due to the mixed geometry. Despite that, it is easy to show that $\mathcal{H}^{\text{MF}}$ cannot give rise to phases with a nonzero Chern number if $\theta = \phi = \varphi = 0$ and tunneling amplitudes $t_\uparrow$ and $t_\downarrow$ are real valued (see Appendix A 2). In order to study TRS breaking due to the NN interaction, we hereafter say that the pseudo spin indices $\uparrow$ and $\downarrow$ are not associated with internal angular momenta but by some other internal states unaffected by time reversal. Subsequently, $\mathcal{H}^{\text{MF}}$ can break TRS only if $(\theta \quad \phi \quad \varphi) \neq (0 \quad 0 \quad 0)$.

III. RESULTS

Figure 2 shows phase diagram for honeycomb-triangular lattice with $U = 5$ and $V = 0$. We used the values $\theta = \phi = \varphi = 0$ because we have numerically verified that this choice yields the lowest grand potential for all values of $\mu_\uparrow$ and $\mu_\downarrow$. Up-spin density is defined as $N_\uparrow/M$, where $N_\uparrow$ and M are the number of $\uparrow$-spin particles and primitive cells in the honeycomb-triangular lattice, respectively. Polarization is defined as $(N_\uparrow - N_\downarrow)/(N_\uparrow + N_\downarrow)$, where $N_\downarrow$ is the number of $\downarrow$-spin particles. By comparing Fig. 2(b) with Fig. 1(d) of Ref. [44], we see that some of the forbidden regions have vanished because Cooper pairs are now allowed to have

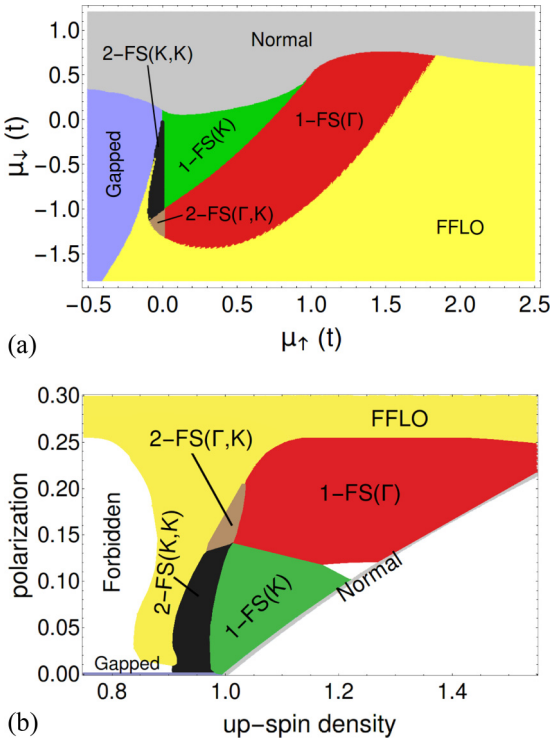

FIG. 2. (Color online) Zero-temperature phase diagram for the honeycomb-triangular lattice with $U = 5$ and $V = 0$. (a) Zero temperature phase diagram for the honeycomb-triangular lattice as a function of chemical potentials $\mu_\uparrow$ and $\mu_\downarrow$. The first two main areas are the normal phase and the FFLO phase, while the rest of the phase diagram is covered by various non-FFLO superfluid phases. (b) Honeycomb-triangular lattice phase diagram as a function of up-spin density and polarization.

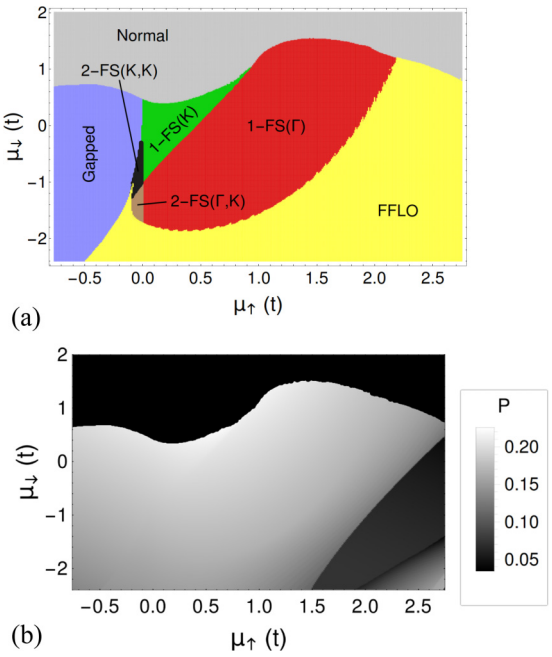

FIG. 3. (Color online) Phases and pairing in the honeycomb-triangular lattice when $U = 5$ and $V = 3$. (a) Zero-temperature phase diagram for the honeycomb-triangular lattice as a function of chemical potentials $\mu_\uparrow$ and $\mu_\downarrow$. The interaction strengths $U = 5$ and $V = 3$. The first two main areas are the normal phase and the FFLO phase, while the rest of the phase diagram is covered by various non-FFLO superfluid phases. (b) Density plot of the relative weight of the NN bond $P = |\Delta_1|/(|\Delta_0| + |\Delta_1|)$ as a function of chemical potentials $\mu_\uparrow$ and $\mu_\downarrow$.

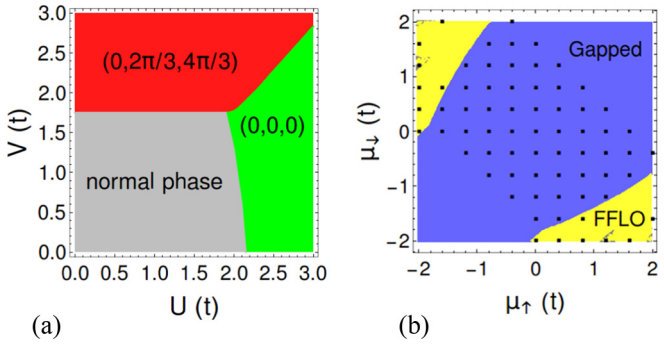

FIG. 4. (Color online) Phase angles in honeycomb-triangular and triangular lattices. (a) Honeycomb-triangular lattice phase angles $(\theta\ \phi\ \varphi)$ at the point $(\mu_\uparrow\ \mu_\downarrow) = (-1.5\ -2.5)$ as a function of on-site and NN interaction strengths U and V. (b) Triangular lattice phase diagram for $U = V = 5$ with $(\theta\ \phi\ \varphi) = (4\pi/3\ \ 2\pi/3\ \ 0)$. Black squares indicate the area where the grand potential is minimized by $(\theta\ \phi\ \varphi) = (4\pi/3\ \ 2\pi/3\ \ 0)$.

nonzero momenta. However, since $\theta = \phi = \varphi = 0$, the phases necessarily have vanishing Chern numbers.

We find that the phase diagrams in Fig. 2 are divided into three main areas. The first two areas are the normal phase and the FFLO superfluid phase, and the third area comprises the rest of the diagram covered by various non-FFLO superfluid phases. The normal phase is simply indicated by vanishing order parameters, i.e., $\Delta_0 = \Delta_1 = 0$. On the other hand, FFLO phase is characterized by $\mathbf{q} \neq 0$ and at least one of the order parameters Δ_0 and Δ_1 being nonzero. The FFLO phase is an unconventional superfluid phase where Cooper pairs have nonzero center-of-mass momenta. Finally, non-FFLO superfluid phase has $\mathbf{q} = 0$ with at least one of the order parameters Δ_0 and Δ_1 being nonzero. The non-FFLO superfluid phase can be further divided into gapless and gapped phases, and the gapless phase can be characterized by the topological arrangement of the one or two Fermi surfaces (Γ centered or K centered). The notation 1-FS(X) means one Fermi surface centered at high symmetry point X and notation 2-FS(X,Y) means two Fermi surfaces centered at high symmetry points X and Y [44].

Figure 3(a) shows the honeycomb-triangular lattice zero temperature phase diagram as a function of $\mu_\uparrow$ and $\mu_\downarrow$ for $U = 5$ and $V = 3$. We used the values $\theta = \phi = \varphi = 0$ because we have numerically verified that this choice yields the lowest grand potential everywhere except in a small region in the lower right corner of the phase diagram. In other words, the system exhibits phase winding in a small region within the FFLO phase. Moreover, Fig. 3(b) shows that there is significant amount of pairing between nearest neighbors when $U = 5$ and $V = 3$. This is very different from the mixed geometry study Ref. [44] in which long-range interactions were not considered. In addition, we find a large area of FFLO, which was not included in the ansatz of Ref. [44]. However, since $\theta = \phi = \varphi = 0$, the phases necessarily have vanishing Chern numbers.

Now, it is of interest to ask whether the system breaks TRS for some values of U, V, $\mu_\uparrow$, and $\mu_\downarrow$. To that end, Fig. 4(a) shows the phase angles θ, ϕ, and φ as a function of U and V at the point $(\mu_\uparrow\ \ \mu_\downarrow) = (-1.5\ \ -2.5)$. Temperature was set to zero. At lower values of U the system is in normal phase if V is small and in superfluid phase with $(\theta\ \ \phi\ \ \varphi) = (0\ \ 2\pi/3\ \ 4\pi/3)$ if V is large. At higher values of U the system is in superfluid phase with $(\theta\ \ \phi\ \ \varphi) = (0\ \ 0\ \ 0)$ if V is small and in superfluid phase with $(\theta\ \ \phi\ \ \varphi) = (0\ \ 2\pi/3\ \ 4\pi/3)$ for large values of V. *Thus the system spontaneously breaks TRS when V becomes large enough.* We also note that the threshold for TRS breaking becomes higher when U is raised. TRS breaking also happens in the triangular lattice [52], but the phase diagram shown in Fig. 4(b) is exceedingly simple compared to the rich phase diagram of Fig. 3(a).

Figure 5 shows the quasiparticle energy bands $E_1(\mathbf{k})$, $E_2(\mathbf{k})$, and $E_3(\mathbf{k})$ along the line Γ-K for the point $(\mu_\uparrow\ \ \mu_\downarrow) = (-1.5\ \ -2.5)$ when $U = 0$ and $V = 3$. The system is in a gapped phase because none of the energy bands cross the Fermi level located at $E_F = 0$. In addition, we note that the two higher bands are degenerate at the Dirac points K because the coupling function $\mathcal{G}_\mathbf{k}$ vanishes at the Dirac points.

We have calculated the Chern numbers by using the method from Ref. [56]. In that method, one obtains the Chern number by summing a gauge-independent field strength $\mathcal{F}_{12}(\mathbf{k}_l)$ over a set of discrete points $\mathbf{k}_l$ covering the entire Brillouin zone. Due to the periodicity of the momentum space Hamiltonian, the Brillouin zone can be regarded as a two-dimensional torus. Remarkably, the field strengths $\mathcal{F}_{12}(\mathbf{k}_l)$ can also be directly measured by using time-of-flight imaging [57]. We

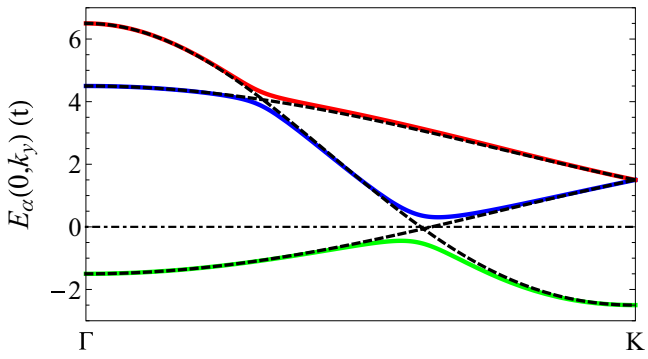

FIG. 5. (Color online) Quasiparticle energy bands $E_\alpha(k_x,k_y)$ on the line Γ-K for interacting (solid) and noninteracting (dashed) systems when $(\mu_\uparrow \quad \mu_\downarrow) = (-1.5 \quad -2.5)$ and $U = 0$ and $V = 3$. Dash-dotted line indicates the Fermi energy $E_F = 0$.

found that the Chern number for the lowest band is $c_3 = 2$. However, the two higher bands do not satisfy the gap opening condition $|E_1 - E_2| \neq 0$ at the Dirac points K. Therefore we did not calculate the Chern numbers for those bands individually, but for the multiplet ψ comprising the two bands. The multiplet Chern number $c_\psi = -2$. Although we have calculated the Chern numbers using periodic boundary conditions, the nonzero Chern numbers still suggest that a finite system with edges would have propagating edge modes [58,59]. The main challenge in detecting such edge modes has been the separation of the small edge-state signal from the bulk background, but Ref. [60] provides a simple and robust way to measure the edge modes. Moreover, when the Fermi energy lies in a gap, the Hall conductance is given by $\sigma_{xy} = -(e^2/h)\sum_n c_n$, where c_n denotes the Chern number of the nth Bloch band and the sum over n is restricted to the bands below the Fermi energy [56,61,62]. The lowest energy band in Fig. 5 is fully below the Fermi energy $E_F = 0$, whereas the two higher bands are completely above the Fermi energy. Consequently, the Hall conductance is $-c_3 = -2$ in units of e^2/h.

IV. DISCUSSION AND SUMMARY

It is remarkable that *simultaneous* occurrence of phase winding and FFLO is possible both in honeycomb-triangular and triangular lattices. In a honeycomb-triangular lattice time-reversal and translational symmetries are simultaneously broken, e.g., at $(\mu_\uparrow \quad \mu_\downarrow) = (2 \quad -2)$ when $U = 0$ and $V = 4$, whereas Fig. 4(b) shows the areas where this happens in a triangular lattice for $U = V = 5$. Although it is known that TRS can be broken in a triangular lattice due to NN interactions [52], we have shown here that *simultaneous* breaking of time-reversal and translational symmetries in the superfluid order parameter of a two-component fermion system may happen both in honeycomb-triangular and triangular lattices.

In summary, the extended Fermi-Hubbard model we have considered in a mixed honeycomb-triangular lattice exhibits a rich phase diagram with gapped and gapless paired phases, as well as spontaneous TRS breaking at NN interaction strengths V higher or equal to the on-site interaction U. The TRS breaking gives rise to topologically nontrivial phases and nonzero Hall conductivity. The connection of our lattice model to various graphene systems [6,63,64] may inspire a search for ways to design mixed geometries on such nanomaterials. Remarkably, we found that TRS breaking happens also in the FFLO state: We thus predict a type of superfluid with simultaneous TRS and translational symmetry breaking. This phase of matter could be realized in the mixed honeycomb-triangular or in the triangular geometry, which are both realizable in ultracold gases, the latter being simpler since it does not require spin-dependent confinement.

ACKNOWLEDGMENTS

We thank D.-H. Kim for useful discussions. This work was supported by the Academy of Finland through its Centres of Excellence Programme (2012–2017) and under Projects No. 263347, No. 251748, and No. 272490 and by the European Research Council (ERC-2013-AdG-340748-CODE). We acknowledge the computational resources provided by Aalto University Science IT project. One of us (R.S.) acknowledges a grant from the University of Oulu.

APPENDIX

1. Geometry of honeycomb-triangular lattice

A mixed-geometry lattice comprising a honeycomb lattice and a triangular lattice has been depicted in Fig. 1(a) and described in detail in the Supplemental Material of Ref. [44]. Following the example of Ref. [44], we take the primitive vectors of the triangular sublattice A to be

$$\mathbf{a}_1 = \left(\frac{\sqrt{3}}{2} \quad \frac{1}{2}\right), \tag{A1}$$

$$\mathbf{a}_2 = \left(\frac{\sqrt{3}}{2} \quad -\frac{1}{2}\right). \tag{A2}$$

The corresponding reciprocal lattice vectors are

$$\mathbf{b}_1 = \left(\frac{2\pi}{\sqrt{3}} \quad 2\pi\right), \tag{A3}$$

$$\mathbf{b}_2 = \left(\frac{2\pi}{\sqrt{3}} \quad -2\pi\right). \tag{A4}$$

The triangular sublattice B is shifted by $(1/\sqrt{3} \quad 0)$ relative to the sublattice A. Thus the A and B sublattices together form a hexagonal lattice.

We impose Born–von Karman boundary conditions on the direct space wave function. That is, we assume that $\psi(\mathbf{r} + N\mathbf{a}_i) = \psi(\mathbf{r})$, where N is a positive integer and $i \in \{1,2\}$. Consequently, allowed momentum values are of the form

$$\mathbf{k} = \frac{m_1\mathbf{b}_1}{N} + \frac{m_2\mathbf{b}_2}{N}, \tag{A5}$$

where $m_1, m_2 \in \mathbb{Z}$ [65]. Thus summations $\sum_{\mathbf{k}}$ run over over such k points that are of the form (A5) and belong to the first Brillouin zone. In each calculation, we used a 400×400 or a 200×200 k-point mesh, depending on the amount of computational work. We solved the eigenvalues of 3×3 matrices by using the method from Ref. [66].

2. Chern number

It is easy to see that matrix $\mathcal{H}_{\mathbf{k}}$ defined in Eq. (9) is symmetric if $t_\uparrow$ and $t_\downarrow$ are real valued and $\theta = \phi = \varphi = 0$. The eigenvectors $|n(\mathbf{k}_l)\rangle$ of a symmetric matrix can always be chosen real valued. Consequently, the link variable $U_\mu(\mathbf{k}_l)$ defined in Eq. (7) of Ref. [56] is equal to unity for all $\mathbf{k}_l$. Subsequently, the lattice field strength $\tilde{F}_{12}(\mathbf{k}_l)$ defined in Eq. (8) of Ref. [56] vanishes for all $\mathbf{k}_l$. It follows that the lattice Chern number $\tilde{c}_n$ defined in Eq. (9) of Ref. [56] vanishes if $t_\uparrow$ and $t_\downarrow$ are real valued and $\theta = \phi = \varphi = 0$.

3. Symmetries of $E_\alpha(\mathbf{k})$ and $n_\sigma(\mathbf{k})$

If the FFLO-momentum $\mathbf{q} = 0$ and $\theta = \phi = \varphi = 0$, the quasiparticle energies $E_\alpha(\mathbf{k})$ and momentum distributions $n_\sigma(\mathbf{k})$ exhibit the symmetries of the underlying triangular lattice. However, if at least one of the phase angles θ, ϕ, and φ is given a nonzero value, $E_\alpha(\mathbf{k})$ and $n_\sigma(\mathbf{k})$ may lose the symmetries of the triangular lattice. Nevertheless, we prove next that $E_\alpha(\mathbf{k})$ and $n_\sigma(\mathbf{k})$ retain the symmetries of the triangular lattice in the case $\Delta_0 = \mathbf{q} = 0$ and $(\theta \quad \phi \quad \varphi) = (0 \quad 2\pi/3 \quad 4\pi/3)$.

Let us say that $\Delta_0 = \mathbf{q} = 0$ and $(\theta \quad \phi \quad \varphi) = (0 \quad 2\pi/3 \quad 4\pi/3)$ and consider how $H_{\mathbf{k}}$ changes when $\mathbf{k}$ is rotated anticlockwise by $\pi/3$. The noninteracting dispersions $\xi_{\mathbf{k}}^{(i)}$ do not change, because they exhibit the symmetries of the underlying triangular lattice. On the other hand, the $\pi/3$ rotation is equivalent to making the cyclic permutation $(\theta \quad \phi \quad \varphi) \to (\phi \quad \varphi \quad \theta)$. That is,

$$(0 \quad 2\pi/3 \quad 4\pi/3) \to (2\pi/3 \quad 4\pi/3 \quad 2\pi), \qquad \text{(A6)}$$

where we have also used the fact that the angles are defined modulo 2π. Thus, the $\pi/3$ rotation amounts to changing the total phase of $\mathcal{G}_{\mathbf{k}}$ by $2\pi/3$. It is easy to see that changing the total phase of $\mathcal{G}_{\mathbf{k}}$ does not affect the eigenvalues of $H_{\mathbf{k}}$, but the phase of the third eigenvector component changes. However, the momentum distributions $n_\sigma(\mathbf{k})$ depend only on the squared norms of the eigenvector components, and therefore both $E_\alpha(\mathbf{k})$ and $n_\sigma(\mathbf{k})$ remain unchanged.

Reflecting vector $\mathbf{k}$ about the x or y axis is equivalent to making the permutation $(\theta \quad \phi \quad \varphi) \to (\phi \quad \theta \quad \varphi)$. That is,

$$(0 \quad 2\pi/3 \quad 4\pi/3) \to (2\pi/3 \quad 0 \quad -2\pi/3), \qquad \text{(A7)}$$

where we have also used the fact that the angles are defined modulo 2π. Thus, reflecting vector $\mathbf{k}$ about the x or y axis is equivalent to making the change $\mathcal{G}_{\mathbf{k}} \to e^{i2\pi/3}\mathcal{G}_{\mathbf{k}}^*$. It is easy to see that this does not affect the eigenvalues of $H_{\mathbf{k}}$, but eigenvectors are complex conjugated and the third eigenvector component is also multiplied by $e^{i2\pi/3}$. However, the momentum distributions $n_\sigma(\mathbf{k})$ depend only on the squared norms of the eigenvector components, and therefore both $E_\alpha(\mathbf{k})$ and $n_\sigma(\mathbf{k})$ remain unchanged.

[1] J. Bardeen, L. N. Cooper, and J. R. Schrieffer, Theory of superconductivity, Phys. Rev. **108**, 1175 (1957).

[2] P. Fulde and R. A. Ferrell, Superconductivity in a strong spin-exchange field, Phys. Rev. **135**, A550 (1964).

[3] A. I. Larkin and Yu. N. Ovchinnikov, Nonuniform state of superconductors, Sov. Phys. JETP **20**, 762 (1965).

[4] B. Jin, Phase diagram and superconducting density of states of the quasi-two-dimensional d-wave superconductor in parallel magnetic field, Europhys. Lett. **72**, 270 (2005).

[5] B. Roy and I. F. Herbut, Unconventional superconductivity on honeycomb lattice: Theory of Kekule order parameter, Phys. Rev. B **82**, 035429 (2010).

[6] R. Nandkishore, L. S. Levitov, and A. V. Chubukov, Chiral superconductivity from repulsive interactions in doped graphene, Nat. Phys. **8**, 158 (2012).

[7] G. E. Volovik, Quantized hall effect in superfluid helium-3 film, Phys. Lett. A **128**, 277 (1988).

[8] M. Sigrist and K. Ueda, Phenomenological theory of unconventional superconductivity, Rev. Mod. Phys. **63**, 239 (1991).

[9] M. Vojta, Y. Zhang, and S. Sachdev, Quantum phase transitions in d-wave superconductors, Phys. Rev. Lett. **85**, 4940 (2000).

[10] A. M. Black-Schaffer, W. Wu, and K. Le Hur, Chiral d-wave superconductivity on the honeycomb lattice close to the Mott state, Phys. Rev. B **90**, 054521 (2014).

[11] C. L. Kane and E. J. Mele, Z_2 topological order and the quantum spin hall effect, Phys. Rev. Lett. **95**, 146802 (2005).

[12] B. A. Bernevig and T. L. Hughes, *Topological Insulators and Topological Superconductors* (Princeton University Press, Princeton, NJ, 2013).

[13] J. Nagamatsu, N. Nakagawa, T. Muranaka, Y. Zenitani, and J. Akimitsu, Superconductivity at 39 K in magnesium diboride, Nature (London) **410**, 63 (2001).

[14] M. R. Norman, Trend: High-temperature superconductivity in the iron pnictides, Physics **1**, 21 (2008).

[15] Y. Kamihara, T. Watanabe, M. Hirano, and H. Hosono, Iron-based layered superconductor La[$O_{1-x}F_x$]FeAs(x = 0.05 − 0.12) with $T_c = 26$ K, J. Am. Chem. Soc. **130**, 3296 (2008).

[16] K. Kuroki, S. Onari, R. Arita, H. Usui, Y. Tanaka, H. Kontani, and H. Aoki, Unconventional pairing originating from the disconnected Fermi surfaces of superconducting LaFeAs$O_{1-x}F_x$, Phys. Rev. Lett. **101**, 087004 (2008).

[17] Z. Huang and X. Hu, Josephson effects in three-band superconductors with broken time-reversal symmetry, Appl. Phys. Lett. **104**, 162602 (2014).

[18] X. Hu and Z. Wang, Stability and Josephson effect of time-reversal-symmetry-broken multicomponent superconductivity induced by frustrated intercomponent coupling, Phys. Rev. B **85**, 064516 (2012).

[19] S. Z. Lin and X. Hu, Massless leggett mode in three-band superconductors with time-reversal-symmetry breaking, Phys. Rev. Lett. **108**, 177005 (2012).

[20] M. Boninsegni and N. V. Prokof'ev, *Colloquium*: Supersolids: What and where are they?, Rev. Mod. Phys. **84**, 759 (2012).

[21] O. Tieleman, O. Dutta, M. Lewenstein, and A. Eckardt, Spontaneous time-reversal symmetry breaking for spinless fermions on a triangular lattice, Phys. Rev. Lett. **110**, 096405 (2013).

[22] C. Salomon, G. Shlyapnikov, and L. Cugliandolo, *Many-Body Physics with Ultracold Gases* (Oxford University Press, Oxford, UK, 2010).

[23] T. Esslinger, Fermi-Hubbard physics with atoms in an optical lattice, Annu. Rev. Condens. Matter Phys. **1**, 129 (2010).

[24] L. He and W. Hofstetter, Supersolid phase of cold fermionic polar molecules in two-dimensional optical lattices, Phys. Rev. A **83**, 053629 (2011).

[25] A. V. Gorshkov, S. R. Manmana, G. Chen, J. Ye, E. Demler, M. D. Lukin, and A. M. Rey, Tunable superfluidity and quantum magnetism with ultracold polar molecules, Phys. Rev. Lett. **107**, 115301 (2011).

[26] S. G. Bhongale, L. Mathey, S.-W. Tsai, C. W. Clark, and E. Zhao, Bond order solid of two-dimensional dipolar fermions, Phys. Rev. Lett. **108**, 145301 (2012).

[27] M. L. Kiesel, C. Platt, and R. Thomale, Unconventional Fermi surface instabilities in the Kagome Hubbard model, Phys. Rev. Lett. **110**, 126405 (2013).

[28] W.-M. Huang, C.-Y. Lai, C. Shi, and S.-W. Tsai, Unconventional superconducting phases for the two-dimensional extended Hubbard model on a square lattice, Phys. Rev. B **88**, 054504 (2013).

[29] A. Griesmaier, J. Werner, S. Hensler, J. Stuhler, and T. Pfau, Bose-Einstein condensation of chromium, Phys. Rev. Lett. **94**, 160401 (2005).

[30] M. Lu, N. Q. Burdick, S. H. Youn, and B. L. Lev, Strongly dipolar Bose-Einstein condensate of dysprosium, Phys. Rev. Lett. **107**, 190401 (2011).

[31] K. Aikawa, A. Frisch, M. Mark, S. Baier, A. Rietzler, R. Grimm, and F. Ferlaino, Bose-Einstein Condensation of erbium, Phys. Rev. Lett. **108**, 210401 (2012).

[32] K.-K. Ni, S. Ospelkaus, M. H. G. de Miranda, A. Pe'er, B. Neyenhuis, J. J. Zirbel, S. Kotochigova, P. S. Julienne, D. S. Jin, and J. Ye, A high phase-space-density gas of polar molecules, Science **322**, 231 (2008).

[33] B. Yan, S. A. Moses, B. Gadway, J. P. Covey, K. R. A. Hazzard, A. M. Rey, D. S. Jin, and J. Ye, Observation of dipolar spin-exchange interactions with lattice-confined polar molecules, Nature (London) **501**, 521 (2013).

[34] K.-K. Ni, S. Ospelkaus, D. Wang, G. Quéméner, B. Neyenhuis, M. H. G. de Miranda, J. L. Bohn, J. Ye, and D. S. Jin, Dipolar collisions of polar molecules in the quantum regime, Nature (London) **464**, 1324 (2010).

[35] M. Saffman, T. G. Walker, and K. Mølmer, Quantum information with Rydberg atoms, Rev. Mod. Phys. **82**, 2313 (2010).

[36] J. Schachenmayer, I. Lesanovsky, A. Micheli, and A. J. Daley, Dynamical crystal creation with polar molecules or Rydberg atoms in optical lattices, New J. Phys. **12**, 103044 (2010).

[37] S. E. Anderson, K. C. Younge, and G. Raithel, Trapping Rydberg atoms in an optical lattice, Phys. Rev. Lett. **107**, 263001 (2011).

[38] P. Schauß, M. Cheneau, M. Endres, T. Fukuhara, S. Hild, A. Omran, T. Pohl, C. Gross, S. Kuhr, and I. Bloch, Observation of spatially ordered structures in a two-dimensional Rydberg gas, Nature (London) **491**, 87 (2012).

[39] L.-K. Lim, A. Lazarides, A. Hemmerich, and C. Morais Smith, Competing pairing states for ultracold fermions in optical lattices with an artificial staggered magnetic field, Phys. Rev. A **82**, 013616 (2010).

[40] P. Soltan-Panahi, J. Struck, P. Hauke, A. Bick, W. Plenkers, G. Meineke, C. Becker, P. Windpassinger, M. Lewenstein, and K. Sengstock, Multi-component quantum gases in spin-dependent hexagonal lattices, Nat. Phys. **7**, 434 (2011).

[41] P. Windpassinger and K. Sengstock, Engineering novel optical lattices, Rep. Prog. Phys. **76**, 086401 (2013).

[42] L. J. LeBlanc and J. H. Thywissen, Species-specific optical lattices, Phys. Rev. A **75**, 053612 (2007).

[43] G. Lamporesi, J. Catani, G. Barontini, Y. Nishida, M. Inguscio, and F. Minardi, Scattering in mixed dimensions with ultracold gases, Phys. Rev. Lett. **104**, 153202 (2010).

[44] D.-H. Kim, J. S. J. Lehikoinen, and P. Törmä, Topological transitions of gapless paired states in mixed-geometry lattices, Phys. Rev. Lett. **110**, 055301 (2013).

[45] S. Kokkelmans, Feshbach resonances in ultracold gases, in *Quantum Gas Experiments*, Cold Atoms, edited by P. Törmä and K. Sengstock, Vol. 3 (Imperial College Press, London, 2014), pp. 63–85.

[46] L. Santos, Dipolar Gases–Theory, in *Quantum Gas Experiments*, Cold Atoms, edited by P. Törmä and K. Sengstock, Vol. 3 (Imperial College Press, London, 2014), pp. 293–309.

[47] E. A. L. Henn, J. Billy, and T. Pfau, Dipolar Gases–Experiment, in *Quantum Gas Experiments*, Cold Atoms, edited by P. Törmä and K. Sengstock, Vol. 3 (Imperial College Press, London, 2014), pp. 311–325.

[48] K. Fossheim and A. Sudbø, *Superconductivity: Physics and Applications* (John Wiley & Sons, New York, 2004).

[49] G. Baskaran, Resonating-valence-bond contribution to superconductivity in MgB_2, Phys. Rev. B **65**, 212505 (2002).

[50] P. W. Anderson, The resonating valence bond state in La_2CuO_4 and superconductivity, Science **235**, 1196 (1987).

[51] When such an FF ansatz minimizes the energy, the actual ground state may be an LO solution of cosine form where the translational symmetry is broken in the amplitude and not only phase of the order parameter. The LO solutions in known cases have lower energies than the FF, and thus FF ground states can be taken as indicators of more general FFLO-type states.

[52] B. Kumar and B. S. Shastry, Superconductivity in CoO_2 layers and the resonating valence bond mean-field theory of the triangular lattice t-J model, Phys. Rev. B **68**, 104508 (2003).

[53] R. Sarjonen, *Large Scattering Lengths and Long-Range Interactions in Ultracold Atomic Gases* (Unigrafia Oy, Helsinki, 2015).

[54] See Sec. IV of Ref. [39] and references therein.

[55] P. Törmä and K. Sengstock (eds.), *Quantum Gas Experiments*, Cold Atoms Vol. 3 (Imperial College Press, London, 2014).

[56] T. Fukui, Y. Hatsugai, and H. Suzuki, Chern numbers in discretized brillouin Zone: Efficient method of computing (spin) hall conductances, J. Phys. Soc. Jpn. **74**, 1674 (2005).

[57] D.-L. Deng, S.-T. Wang, and L.-M. Duan, Direct probe of topological order for cold atoms, Phys. Rev. A **90**, 041601 (2014).

[58] Y. Hatsugai, Edge states in the integer quantum Hall effect and the Riemann surface of the Bloch function, Phys. Rev. B **48**, 11851 (1993).

[59] Y. Hatsugai, Chern number and edge states in the integer quantum Hall effect, Phys. Rev. Lett. **71**, 3697 (1993).

[60] N. Goldman, J. Dalibard, A. Dauphin, F. Gerbier, M. Lewenstein, P. Zoller, and I. B. Spielman, Direct imaging of topological edge states in cold-atom systems, PNAS **110**, 6736 (2013).

[61] D. J. Thouless, M. Kohmoto, M. P. Nightingale, and M. den Nijs, Quantized hall conductance in a two-dimensional periodic potential, Phys. Rev. Lett. **49**, 405 (1982).

[62] M. Kohmoto, Topological invariant and the quantization of the Hall conductance, Ann. Phys. **160**, 343 (1985).

[63] Y. Jiang, D.-X. Yao, E. W. Carlson, H.-D. Chen, and J. P. Hu, Andreev conductance in the $d + id'$-wave superconducting states of graphene, Phys. Rev. B **77**, 235420 (2008).

[64] B. Uchoa and A. H. Castro Neto, Superconducting states of pure and doped graphene, Phys. Rev. Lett. **98**, 146801 (2007).

[65] N. W. Ashcroft and N. D. Mermin, *Solid State Physics* (Saunders College Publishing, Philadelphia, 1976).

[66] J. Kopp, Efficient Numerical diagonalization of Hermitian 3×3 matrices, Int. J. Mod. Phys. C **19**, 523 (2008).